Eur. Phys. J. D **11**, 347–353 (2000)

THE EUROPEAN PHYSICAL JOURNAL D

EDP Sciences

Free electron-positron pair production in collisions of Au^{79+}(10.8 GeV/u) with Cu^{29+}, Ag^{47+} and Au^{79+}

R. Tenzer[a], N. Grün, and W. Scheid[b]

Institut für theoretische Physik Justus-Liebig-Universität Giessen, Germany

Received 21 December 1999 and Received in final form 6 March 2000

Abstract. Total and differential cross-sections for the production of free electron-positron pairs are calculated for the reactions Au^{79+} (10.8 GeV/u) on Cu^{29+}, Ag^{47+} and Au^{79+}. The methods used are the semiclassical approach and the solution of the time-dependent Dirac equation by a coupled channel method with free wavepakets describing the created fermions. The obtained total cross-sections are in good agreement with the experimental data. The differential cross-sections give informations about the correlation between the electron and positron.

PACS. 03.65.Pm Relativistic wave equations – 14.60.Cd Electrons (including positrons) – 34.10.+x General theories and models of atomic and molecular collisions and interactions (including statistical theories, transition state, stochastic and trajectory models, etc.)

1 Introduction

In relativistic heavy ion collisions electron-positron pairs can be produced. We distinguish the production of free and bound-free electron-positron pairs. In the first process the leptons are created in free states. Bound-free pair production means that the electron is captured in a bound state of an ion, while the positron stays free. In this paper we regard only the free pair production process.

It was shown by Greiner *et al.* [1], Thiel *et al.* [2] and Momberger *et al.* [3] that the electron-positron pair production is a non-perturbative process for highly charged ions and small impact parameters. Several calculations exist for the pair production in a non-perturbative formalism. Becker *et al.* [4], Wells *et al.* [5] and Momberger *et al.* [6] solved the time-dependent Dirac equation on a lattice. The difficulty of this method is that, due to computer capacity reasons, the lattice used can not be chosen large enough together with a fine grid size. Momberger *et al.* [7] and Rumrich *et al.* [8] used the coupled channel method for a non-perturbative description. It was shown by Rumrich *et al.* [9] and Baltz *et al.* [10] that the results of coupled channel calculations are gauge dependent, if a finite basis set is applied.

Detailed informations on perturbative and non-perturbative theories for the electron-positron pair production can be found in the review article of Bertulani and Baur [11] and the book of Eichler and Meyerhof [12].

Stimulated by recent experiments of Claytor *et al.* [13] and Belkacem *et al.* [14] on the pair production, we calculate the total and differential pair production cross-section in this paper. In order to interpret experiments of Belkacem [15] we consider reactions with a bare gold nucleus Au^{79+} as projectile with a kinetic energy of 10.8 GeV/u scattered at Au^{79+}, Ag^{47+} and Cu^{29+} ions. Differential cross-sections of pair production should yield more information about the creation process than the total cross-section and would be a detailed test of the theory for correlations in the production process of electron-positron pairs.

In Section 2 of this paper we describe our treatment of the time-dependent Dirac equation with the coupled channel method and give an expression for the correlation between the fermions. Section 3 contains the discretisation of the momentum space with standing wavepakets. Results are shown and discussed in Section 4.

We measure the energy in MeV, the momentum in MeV/c, the time in fm/c and the length in fm. In this units $\hbar$ has the value of 197.3 MeV fm/c. The charge of the electron is denoted by $-e$.

2 Theoretical description

The electron-positron pair production is treated with a semiclassical approach. The nuclear motion and the electromagnetical field are described classically. The colliding ions are assumed to move on straight line trajectories in the xz-plane parallel to the z-axis with constant but opposite velocities $\pm v_0$ ($v_0 > 0$) as shown in Figure 1.

[a] This work is part of the doctoral thesis of Ralf Tenzer, Giessen (D26), 1999.

[b] e-mail: `scheid@theo.physik.uni-giessen.de`

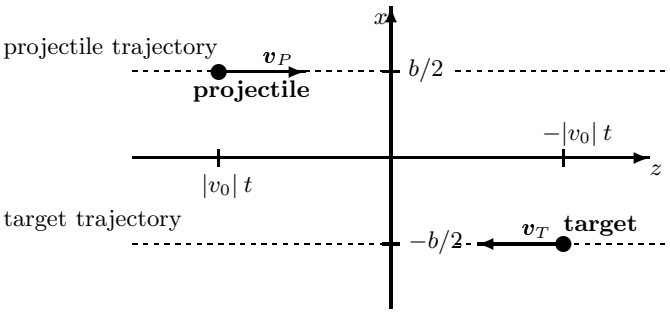

Fig. 1. The ions move in the xz-plane on straight line trajectories parallel to the z-axis with equal speed but opposite velocities with an impact parameter b. The target has the velocity $-|v_0|$ and the x-coordinate $-b/2$ to the z-axis, the projectile the velocity $|v_0|$ and the x-coordinate $b/2$ to the z-axis.

The corresponding coordinate system is denoted as equal-speed system. The connection between the Lorentz-factors of the laboratory frame, where the target nucleus is fixed, and of the equal-speed system is

$$\gamma_{\rm Lab} = 2\gamma^2 - 1. \tag{1}$$

The labels "target" and "projectile" are arbitrary in the equal-speed system, but they help to distinguish between the two ions. The trajectories are given by

$$\mathbf{R}_{\rm T,P}(t) = \mp(\frac{b}{2}\,\mathbf{e}_x + v_0 t\,\mathbf{e}_z), \tag{2}$$

with the impact parameter b. Here and in the following the indices T and P stand for the target and projectile. The electromagnetic fields of the ions are given by the Liénard-Wiechert-potentials (upper sign for the target and lower sign for the projectile with charge numbers $Z^{\rm T}$ and $Z^{\rm P}$, respectively)

$$A_\mu(x) = A^{\rm T}_\mu(x) + A^{\rm P}_\mu(x) \tag{3}$$

$$A^{\rm T,P}_\mu(x) = \gamma\frac{Z^{\rm T,P}e}{4\pi}\;(1,0,0,\mp\frac{v_0}{c})\;\frac{1}{r'_{\rm T,P}} \tag{4}$$

with

$$r'_{\rm T,P} = \sqrt{(x \pm \frac{b}{2})^2 + y^2 + \gamma^2(z \pm v_0 t)^2} \tag{5}$$

and the four vector $x = (ct, \mathbf{r})$.

The time-development of the lepton-field operator Ψ is given by

$$\mathrm{i}\hbar\frac{\partial}{\partial t}\Psi(x) = (H_0 + H_{\rm I})\Psi(x) \tag{6}$$

with

$$H_0 = c\boldsymbol{\alpha}\cdot\mathbf{p} + \beta m_0 c^2, \tag{7}$$

$$H_{\rm I} = H^{\rm T}_{\rm I} + H^{\rm P}_{\rm I}. \tag{8}$$

With equation (4) we get

$$H^{\rm T,P}_{\rm I} = -\gamma\frac{Z^{\rm T,P}e^2}{4\pi}\;(\mathbb{1} \mp \frac{v_0}{c}\alpha_z)\;\frac{1}{r'_{\rm T,P}}\,. \tag{9}$$

We take the fields of both ions as a perturbation. We start with the expansion of the field operator in free orthonormal discrete states which approximate the positive and negative continuum, φ^0_q and χ^0_q,

$$\Psi(x) = \sum_{q>F} a_q(t)\;\varphi^0_q(x) + \sum_{q<F} c^+_q(t)\;\chi^0_q(x). \tag{10}$$

The Fermi level is $F = -m_0c^2$ and $|F\rangle$ presents the vacuum state. The index q characterizes a state with momentum $\mathbf{p}_q$ and spin quantum number s_q. The operators a_q and c^+_q are time-dependent and fulfill the anticommutation relations

$$\{a_q(t), a^+_{q'}(t)\} = \delta_{qq'}, \quad \{c_q(t), c^+_{q'}(t)\} = \delta_{qq'}. \tag{11}$$

$$\{a_q(t), c_{q'}(t)\} = \{a_q(t), c^+_{q'}(t)\} = 0. \tag{12}$$

The operators a_q, a^+_q and c_q, c^+_q are annihilation and creation operators of free particles in the states φ^0_q and χ^0_q, respectively. For the initial time $t = -\infty$ we have

$$a_q(t=-\infty)|F\rangle = c_q(t=-\infty)|F\rangle = 0, \tag{13}$$

which expresses the fact that no particles are originally present in the vacuum.

We get the number of produced particles with the vacuum expectation value of the particle number operator, *e.g.* for an electron in the state "e":

$$N_e(t) = \langle F|a^+_e(t)\;a_e(t)|F\rangle. \tag{14}$$

We have to know the time behaviour of the creation and annihilation operators, if we want to evaluate the vacuum expectation value at all times and especially for $t \to +\infty$. A second representation of the field operator (10) is obtained by an expansion with time-dependent solutions of the Dirac equation (6)

$$\Psi(x) = \sum_{q>F} b_q\;\varphi_q(x) + \sum_{q<F} d^+_q\;\chi_q(x). \tag{15}$$

The wavefunctions φ_q and χ_q describe the dynamics of the electron states in the field of the ions. The operators b_q and d^+_q are time-independent and fulfill the same anticommutation relations as a_q and c^+_q. The difference between the time-dependent and time-independent operators is, that a_q and c^+_q annihilate and create free states, while b_q and d^+_q do this with the exact solutions of the Dirac equation (6). Relations between these operators can be found from the asymptotic behaviour in time. Asymptotically, for $t \to -\infty$, we demand

$$\varphi_q(x) \overset{t\to-\infty}{\longrightarrow} \varphi^0_q(x), \quad \chi_q(x) \overset{t\to-\infty}{\longrightarrow} \chi^0_q(x). \tag{16}$$

These relations constitute the initial conditions for the time-integration of the wave functions $\varphi_q(x)$ and $\chi_q(x)$

with the Dirac equation (6). A comparison of the two expansions of the field operator (10) and (15) yields for the operators

$$a_q(t) \overset{t\to-\infty}{\longrightarrow} b_q, \quad c_q^+(t) \overset{t\to-\infty}{\longrightarrow} d_q^+. \tag{17}$$

Since we know the asymptotic action of the time-dependent operators, we find for the time-independent operators at all times

$$b_q|F\rangle = 0, \quad d_q|F\rangle = 0. \tag{18}$$

Now we expand φ_r and χ_r in the free states φ_q^0 and χ_q^0

$$\varphi_r(x) = \sum_{q>F} \alpha_{qr}(t)\varphi_q^0(x) + \sum_{q<F} \alpha_{qr}(t)\chi_q^0(x), \quad r > F \tag{19}$$

$$\chi_r(x) = \sum_{q>F} \alpha_{qr}(t)\varphi_q^0(x) + \sum_{q<F} \alpha_{qr}(t)\chi_q^0(x), \quad r < F. \tag{20}$$

Note that the range for the indices q and r defines the interpretation of the coefficients $\alpha_{qr}(t)$. We insert the expansions of φ_r and χ_r into equation (15) and compare the result with equation (10). This leads to the following relation between the time-dependent and time-independent operators

$$a_q(t) = \sum_{r>F} \alpha_{qr}(t)\ b_r + \sum_{r<F} \alpha_{qr}(t)\ d_r^+, \quad q > F \tag{21}$$

$$c_q^+(t) = \sum_{r>F} \alpha_{qr}(t)\ b_r + \sum_{r<F} \alpha_{qr}(t)\ d_r^+, \quad q < F. \tag{22}$$

The time behaviour of the expansion coefficients α_{qr} is obtained from the Dirac equation (6). For instance, if we insert equation (20) into equation (6), we get for $r < F$

$$\mathrm{i}\hbar\frac{\partial}{\partial t}\chi_r(x) = (H_0 + H_\mathrm{I})\chi_r(x) \tag{23}$$

$$\text{l.h.s.: } \mathrm{i}\hbar\Big[\sum_{q>F}\big\{\dot\alpha_{qr}(t)\varphi_q^0(x) + \alpha_{qr}(t)\dot\varphi_q^0(x)\big\} + \sum_{q<F}\big\{\dot\alpha_{qr}(t)\chi_q^0(x) + \alpha_{qr}(x)\dot\chi_q^0(t)\big\}\Big] \tag{24}$$

$$\text{r.h.s.: } (H_0 + H_\mathrm{I})\Big[\sum_{q>F} \alpha_{qr}(t)\varphi_q^0(x) + \sum_{q<F} \alpha_{qr}(t)\chi_q^0(x)\Big]. \tag{25}$$

Since φ_q^0 and χ_q^0 solve the free Dirac equation, we obtain a system of coupled channel equations for the expansion coefficients $\alpha_{sr}(t)$ with $r < F$ after projection with φ_s^0 and χ_s^0:

$$\mathrm{i}\hbar\dot\alpha_{sr}(t) = \sum_{q>F}\langle\varphi_s^0(x)|H_\mathrm{I}|\varphi_q^0(x)\rangle\alpha_{qr}(t) + \sum_{q<F}\langle\varphi_s^0(x)|H_\mathrm{I}|\chi_q^0(x)\rangle\alpha_{qr}(t), \quad s > F,\ r < F, \tag{26}$$

$$\mathrm{i}\hbar\dot\alpha_{sr}(t) = \sum_{q>F}\langle\chi_s^0(x)|H_\mathrm{I}|\varphi_q^0(x)\rangle\alpha_{qr}(t) + \sum_{q<F}\langle\chi_s^0(x)|H_\mathrm{I}|\chi_q^0(x)\rangle\alpha_{qr}(t), \quad s, r < F. \tag{27}$$

A similar system of coupled equations can be derived for $\alpha_{sr}(t)$ with $r > F$. Since all interesting physical quantities may already be expressed by $\alpha_{sr}(t)$ with $r < F$, it is sufficient to solve equations (26, 27).

The initial conditions of the coefficients of the coupled channel system can be inferred from equation (17) to be

$$\alpha_{qr}(t \to -\infty) = \delta_{qr} \quad \text{with} \quad r < F \text{ for all } q. \tag{28}$$

The interesting vacuum expectation values can be expressed in terms of the coefficients α_{qr} $(r < F)$. For the number of produced electrons in a state φ_e^0 (Eq. (14)) we have

$$\begin{aligned} N_e(t) &= \langle F|a_e^+(t)\ a_e(t)|F\rangle \\ &= \langle F|\Big[\sum_{r>F}\alpha_{er}^*(t)\ b_r^+ + \sum_{r<F}\alpha_{er}^*(t)\ d_r\Big] \\ &\quad\times\Big[\sum_{r'>F}\alpha_{er'}(t)\ b_{r'} + \sum_{r'<F}\alpha_{er'}(t)\ d_{r'}^+\Big]|F\rangle \\ &= \sum_{r<F}|\alpha_{er}(t)|^2 \quad \text{with } e > F. \end{aligned} \tag{29}$$

In the same way we calculate the number of produced electron-positron pairs with the electron in state e and the positron in state p

$$\begin{aligned} N_{ep}(t) &= \langle F|a_e^+(t)\ a_e(t)\ c_p^+(t)\ c_p(t)|F\rangle \\ &\ \ \vdots \\ &= N_e(t)\ N_p(t) + |\sum_{r<F}\alpha_{er}^*(t)\ \alpha_{pr}(t)|^2 \\ &\qquad\qquad \text{with } e > F \text{ and } p < F. \end{aligned} \tag{30}$$

The correlation of an electron in state "e" and a positron in state "p" may be defined as

$$\begin{aligned} N_{ep}^\mathrm{corr}(t) &= N_{ep}(t) - N_e(t)\ N_p(t) \\ &= |\sum_{r<F}\alpha_{er}^*(t)\,\alpha_{pr}(t)|^2, \quad e > F,\ p < F. \end{aligned} \tag{31}$$

The product of the expectation values N_e and N_p is the uncorrelated probability to find a pair in a state with the quantum numbers e and p.

3 Discretisation of the continuum

For the representation of a discrete continuum we proceed as follows. We divide the momentum space in cubes with the volume Δ^3P. Figure 2 shows the devision of the momentum space with a maximum momentum of 3 MeV/c. All cubes with their center in the sphere with the radius of 3 MeV/c belong to this basis set. To each cube we attribute standing wavepakets of free states [16,17] of the positive and negative continuum with a momentum $\mathbf{p}_q$, an energy E_q and with both spin possibilities. For instance

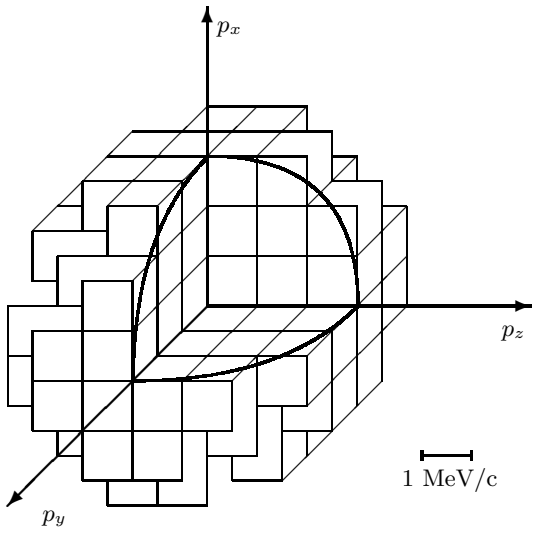

Fig. 2. Discretisation of the momentum space in equal cubes. The radius of the momentum sphere determines the maximum momentum of the states of the basis set.

the standing wavepaket of a positive continuum state is

$$\varphi_q^0(x) = \frac{1}{\sqrt{(2\pi\hbar)^3 \Delta^3 P}} \sqrt{\frac{m_0 c^2}{E_q}}\, u(p_q, s_q) \times \mathrm{e}^{-\mathrm{i}E_q t/\hbar}\, \mathrm{e}^{\mathrm{i}\mathbf{p}_q\cdot\mathbf{x}/\hbar} \int\limits_{\Delta^3 P} \mathrm{d}^3 p\, \mathrm{e}^{\mathrm{i}\mathbf{p}\cdot\mathbf{x}/\hbar}. \quad (32)$$

The difference to moving wavepakets, also called Weyl wavepakets, is, that we extract an energy and a spinor corresponding to the center point of the cube out of the momentum integral. This is a good approximation for small cubes and allows us to calculate the transition matrix elements in the coupled channel equations nearly analytically. However the standing wavepakets do not solve the free Dirac equation exactly. We obtain

$$\mathrm{i}\hbar \frac{\partial}{\partial t} \varphi_q^0(x) = H_0\ \varphi_q^0(x) - F_q(x) \quad (33)$$

with an error term

$$F_q(x) = \frac{c}{\sqrt{(2\pi\hbar)^3 \Delta^3 P}} \sqrt{\frac{m_0 c^2}{E_q}}\, u(p_q, s_q) \times \mathrm{e}^{-\mathrm{i}E_q t/\hbar}\, \mathrm{e}^{\mathrm{i}\mathbf{p}_q\cdot\mathbf{x}/\hbar} \int\limits_{\Delta^3 P} \mathrm{d}^3 p\, \boldsymbol{\alpha}\cdot\mathbf{p}\, \mathrm{e}^{\mathrm{i}\mathbf{p}\cdot\mathbf{x}/\hbar}. \quad (34)$$

In our calculations we may completely neglect this term. In the derivation of the coupled channel equations (26, 27) the error term does not contribute.

Table 1. Total cross-sections (in barn) for the free pair production in collisions of Au^{79+} (10.8 GeV/u) on Cu^{29+}, Ag^{47+} and Au^{79+}. The experimental data were given to us by Belkacem [15]. The results of Becker *et al.* [18] and Ionescu and Eichler [19] were calculated in first order perturbation theory, those of Eby [20] in second order perturbation theory.

collision system	experiment	this work	Becker	Ionescu	Eby
Au^{79+} + Cu^{29+}	42	43.44	12	15	23
Au^{79+} + Ag^{47+}	85	92.21	31	40	59
Au^{79+} + Au^{79+}	180	211.98	87	113	167

4 Results and discussion

We report on calculations for the symmetric system Au^{79+} on Au^{79+} and the asymmetric systems Au^{79+} on Ag^{47+} and Au^{79+} on Cu^{29+} with the kinetic energy of the gold projectile of 10.8 GeV/u in the laboratory frame on fixed targets. The states of the basis set used have a maximum momentum of 3 MeV/c and the width ΔP of the channels is 1 MeV/c (see Fig. 2). These parameters describe a basis set with 544 free states. The calculation of a collision with fixed impact parameter and energy requires 2.5 hours on a vector computer. The presented results are obtained by integrating over the impact parameter.

4.1 Total cross-sections

We calculated the total cross-section for the free pair production for bare gold ions with a kinetic energy of 10.8 GeV/u on bare copper, silver and gold ions. The results are shown in Table 1. The second column contains the experimental results of Belkacem [15]. Our calculations in the third column are in good agreement with the experimental values. The next three columns give results obtained in lowest order perturbation theory. Becker *et al.* [18] apply exact Dirac wavefunctions of the target for their perturbation calculations. Their method is restricted by a slow convergence behaviour of a multipole expansion to γ values not too high, but is still applicable in our case at $\gamma_{\mathrm{FT}} = 12.6$ (FT stands for fixed target). Ionescu and Eichler [19] use Sommerfeld-Maue functions for the target continuum states. This approximation should be taken with care for lower continuum energies of the produced pairs where, at least still for $\gamma_{\mathrm{FT}} = 12.6$, the cross-sections differential in the produced particles are large. The last column is extracted from the paper of Eby [20], who completed the early work of Racah [21]. They use free Dirac waves and the fields of both nuclei, projectile and target, as perturbation. Correspondingly the lowest order perturbation is the second order, as it is also the case with the free wavepackets of this paper. The perturbative results underestimate the experimental cross-sections. This behaviour is a signature for the non-perturbative character of the free pair production at small impact parameters.

We should mention that, within our finite basis set, perturbative calculations are easy to perform by solving the coupled channel equations successively. This has been

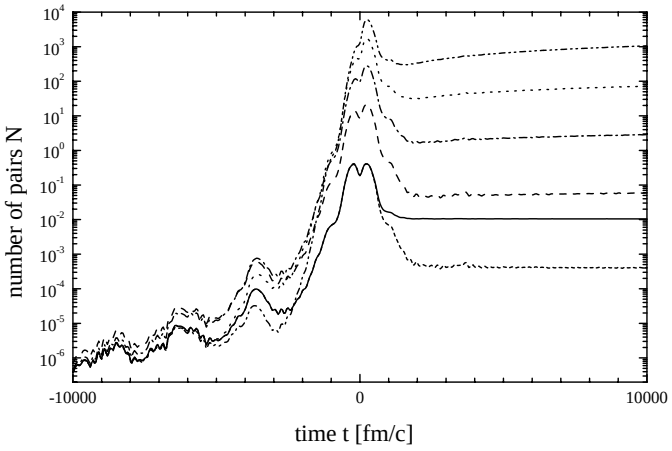

Fig. 3. Time development of the created electron positron pairs in Au^{79+} (10.8 GeV/u) on Au^{79+} collisions at an impact parameter $b = 386$ fm, obtained in first order perturbation theory (lowest curve), by coupled channel calculations (solid curve) and in second, third, fourth and fifth order perturbation theory (upper curves). The first order calculation should in principle vanish for $t \to \infty$. The remaining value of 4×10^{-4} is the error of this calculation.

done for the given collision systems. The outcome is, that at small impact parameters of *e.g.* 386 fm (the Compton wave length of the electron), the next orders of perturbation calculations deviate more and more from the fully coupled channel result, and only for orders, which are hopeless to consider with exact perturbation calculations, this trend is reversed. Figure 3 shows this behaviour for Au^{79+} on Au^{79+} at 10.8 GeV/u at an impact parameter of $b = 386$ fm.

4.2 Differential angular distributions and correlations

Figures 4 and 5 show the angular distribution of the produced electrons and positrons for the symmetric system Au^{79+} on Au^{79+} (Fig. 4) and the asymmetric system Au^{79+} on Cu^{79+} (Fig. 5) as a function of the emission angle ϑ with respect to the positive z-axis. The discretisation of the momentum space limits our resolution in the angle. In the histograms the emission of electrons and positrons is collected in bins of $\Delta\vartheta = 15°$. The collision system Au^{79+} on Au^{79+} (Fig. 4) shows a symmetric distribution both for the electrons and positrons. The produced fermions prefer to leave the creation zone under an angle of about 50° to the trajectories of the ions. We note that in our system of reference the value of γ is 2.6. Higher γ values would lead to more pronounced angular distributions in the forward direction. We see the same behaviour in the system Au^{79+} on Cu^{29+} (Fig. 5), but the distribution is now asymmetric. Smaller angles seem to be favoured.

Now we examine the correlation between the emission angles of the produced fermions. The difference angle ϑ_{pe} is defined as the angle between the momentum vectors of the positron and electron. The corresponding differential cross-section is $d\sigma(\vartheta_{pe})/d\vartheta_{pe}$. Just as before, the resolution of the difference angle is limited by the discretisation

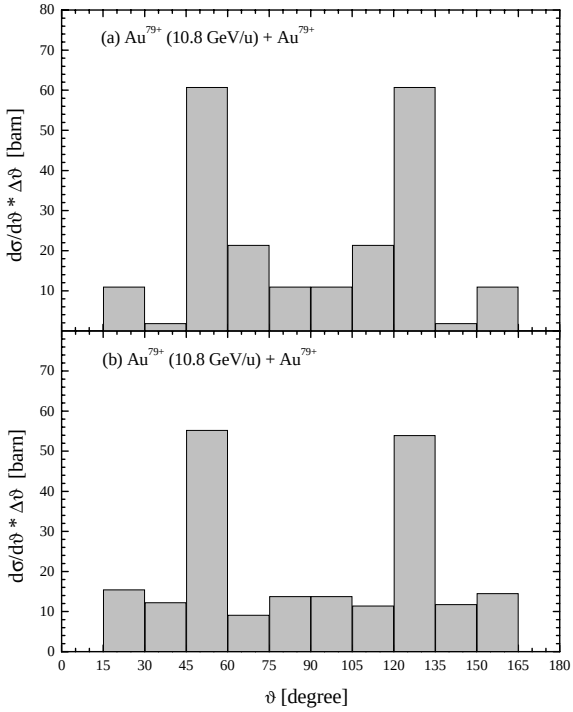

Fig. 4. The angular distributions of the produced electrons (a) and positrons (b) in the collision Au^{79+} (10.8 GeV/u) on Au^{79+} are shown. The gold projectile moves parallel to the positive z-axis. The angle ϑ is defined with respect to the positive z-axis.

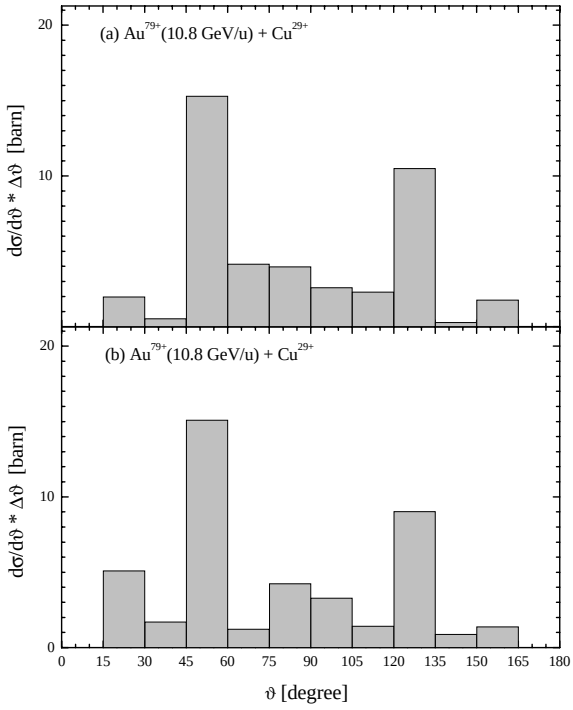

Fig. 5. The angular distributions of the produced electrons (a) and positrons (b) in the collision Au^{79+} (10.8 GeV/u) on Cu^{29+} are shown. The gold projectile moves parallel to the positive z-axis. The angle ϑ is defined with respect to the positive z-axis.

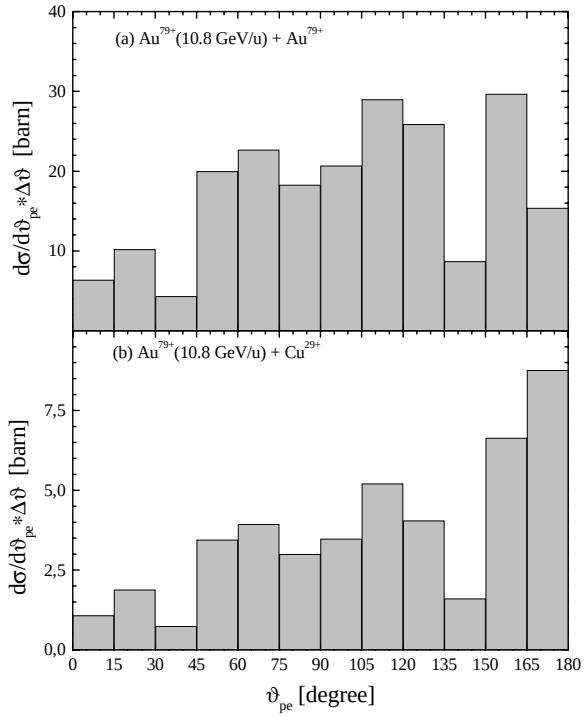

Fig. 6. The differential cross-section $\mathrm{d}\sigma/\mathrm{d}\vartheta_{pe}$ of the difference angle ϑ_{pe} between the produced positron and electron is plotted for (a) Au^{79+} (10.8 GeV/u) + Au^{79+} and (b) Au^{79+} (10.8 GeV/u) + Cu^{29+} ($\Delta\vartheta = 15°$).

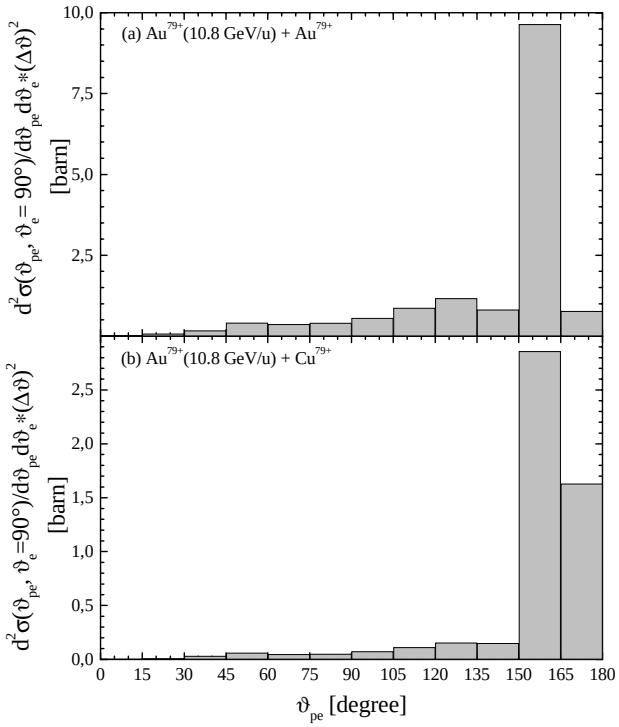

Fig. 7. The double differential cross-section $\mathrm{d}^2\sigma(\vartheta_{pe}, \vartheta_e = 90°)/(\mathrm{d}\vartheta_{pe}\mathrm{d}\vartheta_e)$ for electrons emitted transversal to the ion trajectories is plotted against the difference angle ϑ_{pe} between the positron and electron. (a) Au^{79+} (10.8 GeV/u) + Au^{79+} and (b) Au^{79+} (10.8 GeV/u) + Cu^{29+} ($\Delta\vartheta = 15°$).

of the momentum space. In Figure 6 a histogram of the differential cross-section $\mathrm{d}\sigma/\mathrm{d}\vartheta_{pe}$ is plotted for a symmetric and asymmetric system. The distributions of both systems are similar. The angular distribution is relatively broad. Some tendency for angles around 90° may be extracted. In the asymmetric system large angles are preferred slightly.

Figures 7 and 8 show histograms of the double differential cross-sections $\mathrm{d}^2\sigma/(\mathrm{d}\vartheta_{pe}\mathrm{d}\vartheta_e)$ where ϑ_{pe} is the difference angle between the emission directions of the positron and electron and ϑ_e the emission angle of the electron. The emission angle is chosen $\vartheta_e = 90°$ (Fig. 7) and $\vartheta_e = 0°$ (Fig. 8), *i.e.* transversal and parallel to the trajectories of the ions. If the electron is emitted transversal, the positron leaves nearly in the opposite direction (see Fig. 7). The difference angle between the positron and electron is mainly around 160°. The reason, that the positron does not move in exactly the opposite direction (difference angle 180°), is due to the push of the positron by the positive ion. At first glance the figures for the symmetric case (Fig. 7a) and the asymmetric one (Fig. 7b) are very similar. But for large angles there is a large difference. In the Au^{79+} on Au^{79+} collision the angle area around 180° is nearly empty compared to the angle area around 160°. This is not the case for the Au^{79+} on Cu^{29+} system. The repulsion of the copper ion is much weaker than the one of the gold ion allowing the positron to move opposite to the electron.

Finally in Figure 8 we show the situation for the electrons being emitted parallel to the direction of the ions. There is no large difference between the symmetric and

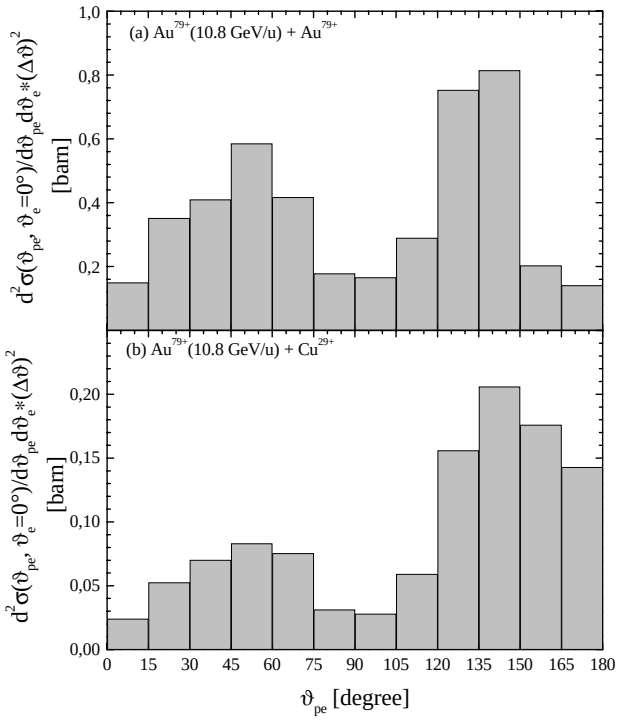

Fig. 8. The double differential cross-section $\mathrm{d}^2\sigma(\vartheta_{pe}, \vartheta_e = 0°)/(\mathrm{d}\vartheta_{pe}\mathrm{d}\vartheta_e)$ for electrons emitted parallel to the ion trajectories is plotted against the difference angle ϑ_{pe} between the positron and electron. (a) Au^{79+} (10.8 GeV/u) + Au^{79+} and (b) Au^{79+} (10.8 GeV/u) + Cu^{29+} ($\Delta\vartheta = 15°$).

asymmetric collision cases. The positrons prefer difference angles around 45° and 135°. The numbers on the ordinate scale show that the probability for "longitudinal" electrons is smaller than for "transversal" electrons.

5 Final remarks

Though it is not the topic of this paper, we would like to add some remarks on the process of electron capture from pair production. First, the published experimental results for the same collision systems [14], treated in this paper, are by more than a factor of magnitude lower than the free-free cross-section. Second, the perturbative calculations of Becker *et al.* [22] roughly agree with the experiment. Thus, it seems that the free-free pair process is nonperturbative at the given experimental conditions whereas the free-bound process is already perturbative. The reason is not quite clear and the question cannot be finally answered without nonperturbative calculations for the free-bound process. Such calculations have been done by Rumrich *et al.* [8] for much lower collision energies of 1.2 GeV/u for the Pb+Pb system. There in fact, the cross-section of the coupled channel calculation is 1.48 b in comparison to 0.30 b in perturbation theory. The experiment of Belkacem *et al.* [23] with U^{92+} on Au at 0.96 GeV/u yielded a cross-section of 2.19 b which is in the order of the nonperturbative result. The screening of the target nucleus by the target electrons has not be considered in the perturbation calculations mentioned above. Although this effect should not be extremely large at 10.8 GeV/u, its outcome would be a suppression of the perturbative results, possibly below the experiment.

Some questions could arise about the maximum momentum of 3 MeV/c used in the calculations and about the packet width of 1 MeV/c. Again one should mention that, in the equal speed system used, the γ values for the nuclei are 2.6 and, therefore, the momenta of the leptons do not exceed a value of $m_o\gamma c = 1.3$ MeV/c by far. Further, we made sure in test calculations that the dependence of the creation probabilities on the lepton energies (or momenta) decreases rapidly with the energy (or momentum) of the leptons. Because of the much higher computational effort by taking a packet width of 0.5 MeV/c, we only carried out a calculation for the Au+Au system at an impact parameter $b = 386$ fm with this higher accuracy and found that our results could be in error of maximally 50% for small impact parameters. In view of this result and the remarks on the perturbation theory already mentioned, we must conclude that the method given in this paper is promising, but a definite answer may need a new computer generation.

The authors thank Dr. A. Belkacem and his coworkers for providing them with the unpublished data of Au^{79+} (10.8 GeV/u) on Cu^{29+}, Ag^{47+} and Au^{79+}. This work was supported by BMBF 06GI847 and the GSI (Darmstadt). The calculations were done at the HLRZ (KFA Jülich), the HRZ in Giessen and the HRZ in Darmstadt.

References

1. W. Greiner, B. Müller, J. Rafelski, *Quantum Electrodynamics of strong fields* (Oxford University Press, Oxford, 1995).
2. J. Thiel, A. Bunker, K. Momberger, N. Grün, W. Scheid, Phys. Rev. A **46**, 2607 (1992).
3. K. Momberger, N. Grün, W. Scheid, J. Phys. B **26**, 1851 (1993).
4. U. Becker, N. Grün, W. Scheid, G. Soff, Phys. Rev. Lett. **56**, 2016 (1986).
5. J.C. Wells, V.E. Oberacker, A.S. Umar, C. Bottcher, M.R. Strayer, J.-S. Wu, G. Plunien, Phys. Rev. A **45**, 6296 (1992).
6. K. Momberger, A. Belkacem, A.H. Sørensen, Phys. Rev. A **53**, 1605 (1996).
7. K. Momberger, N. Grün, W. Scheid, Z. Phys. D **18**, 133 (1991).
8. K. Rumrich, K. Momberger, G. Soff, W. Greiner, N. Grün, W. Scheid, Phys. Rev. Lett. **66**, 2613 (1991).
9. K. Rumrich, W. Greiner, G. Soff, Phys. Lett. A **149**, 17 (1990).
10. A.J. Baltz, M.J. Rhoades-Brown, J. Weneser, Phys. Rev. A **48**, 2002 (1993).
11. C.A. Bertulani, G. Baur, Phys. Rep. **163**, 299 (1988).
12. J. Eichler, W.E. Meyerhof, *Relativistic Atomic Collisions* (Academic Press, San Diego, 1995).
13. N. Claytor, A. Belkacem, T. Dinneen, B. Feinberg, H. Gould, Phys. Rev. A **55**, R842 (1997).
14. A. Belkacem, N. Claytor, T. Dinneen, B. Feinberg, H. Gould, Phys. Rev. A **58**, 1253 (1998).
15. A. Belkacem, results unpublished, private communication.
16. G. Mehler, T. de Reus, U. Müller, J. Reinhardt, B. Müller, W. Greiner, G. Soff, Nucl. Instrum. Meth. A **240**, 559 (1985).
17. G. Mehler, G. Soff, K. Rumrich, W. Greiner, Z. Phys. D **13**, 193 (1989).
18. U. Becker, N. Grün, W. Scheid, J. Phys. B **20**, 1347 (1986).
19. D.C. Ionescu, J. Eichler, Phys. Rev. A **48**, 1176 (1993).
20. P.B. Eby, Phys. Rev. A **39**, 2374 (1989); *ibid.* A **43**, 2258 (1991).
21. G. Racah, Nuovo Cimento **14**, 93 (1937).
22. U. Becker, N. Grün, W. Scheid, J. Phys. B **20**, 2075 (1987).
23. A. Belkacem, H. Gould, B. Feinberg, R. Bossingham, W.E. Meyerhof, Phys. Rev. Lett. **71**, 1514 (1993).